SCIENTIFIC REPORTS

OPEN

SUBJECT AREAS:
NANOWIRES
FUEL CELLS
SYNTHESIS AND PROCESSING
NANOMETROLOGY

Received
9 January 2013

Accepted
14 March 2013

Published
10 April 2013

Correspondence and requests for materials should be addressed to J.-P.A. (jpahn@kist.re.kr)

Polycrystalline nanowires of gadolinium-doped ceria via random alignment mediated by supercritical carbon dioxide

Sang Woo Kim[1] & Jae-Pyoung Ahn[2]

[1]Clean Energy Research Center, Korea Institute of Science and Technology, Seoul 136-791, Republic of Korea, [2]Advanced Analysis Center, Korea Institute of Science and Technology, Seoul 136-791, Republic of Korea.

This study proposes a seed/template-free method that affords high-purity semiconducting nanowires from nanoclusters, which act as basic building blocks for nanomaterials, under supercritical CO_2 fluid. Polycrystalline nanowires of Gd-doped ceria (Gd-CeO_2) were formed by CO_2-mediated non-oriented attachment of the nanoclusters resulting from the dissociation of single-crystalline aggregates. The unique formation mechanism underlying this morphological transition may be exploited for the facile growth of high-purity polycrystalline nanowires.

Ceria (cerium oxide) has been extensively applied in fuel cells[1,2], solid media for chemical mechanical planarization[3], sensors[4], three-way catalysts for the elimination of toxic vehicular exhaust gases[5], and other catalysts[6,7]. Nanostructured CeO_2 possesses a high surface-to-volume ratio that has been exploited for improving redox properties and transport properties. In this light, numerous studies have focused on manufacturing CeO_2 nanomaterials[8,9]. Seeds[10,11] and organic templates[12–15] are typically used to fabricate semiconducting nanowires[16–18], which find applications in nanodevices[10,16,19–21], photonic devices[10,22], nanosensors[23,24], solar cells[25–27], and catalysts[28,29]. However, residual seeds/templates in the nanowires may act as contaminants[10,12] and degrade the material properties. As a result, there is a pressing need to develop nanowire growth techniques that do not involve the use of seeds/templates and still allow for easy manipulation of the material properties and dimensions and facilitate large-scale production. In this regard, methods based on supercritical fluid technology may be advantageous because they allow for deagglomeration[30] and afford defect-free nanowires in high yields with excellent chemical flexibility and synthetic tenability[31,32]. Single-crystalline semiconducting nanowires[10,13,33–35] can grow via a metal-catalyzed[11], vapor-solid[27], oxide-assisted[10,13], or self-assembly mechanism[13] and under supercritical fluid[30–32] conditions. Single-crystalline nanowires in supercritical fluids are generally grown from catalyst seeds or by the oriented attachment of nanoparticles onto specific planes capped with dendrimers or hyperbranched molecules. We have previously fabricated unique polycrystalline CeO_2 nanowires in a specific supercritical fluid region without using functional capping agents or catalyst seeds[36]. However, the mechanism underlying the nucleation and growth of such polycrystalline nanowires could not be elucidated by conventional theories[10,13,33–35]. In the present study, we fabricated randomly oriented polycrystalline 20 mol% Gd-CeO_2 nanowires by a seed-free method using a supercritical CO_2-alcohol co-solvent system and revealed the growth mechanism through detailed panoramic microscopy images.

Results

Morphological evolution of Gd-CeO_2 nanomaterials. The P-T map in Fig. 1, which is experimentally classified by SEM and TEM observations, can be divided into three distinct regions—Regions 1, 2, and 3—corresponding to the morphology of the synthesized Gd-CeO_2 nanomaterials on the basis of temperature and pressure. The SEM and TEM images corresponding to each region (Figs. 2a–d) revealed the morphological evolution from nanoclusters (Region 1) to nanowires (Region 3) via the formation of aggregates (diameter: ~250 nm) (Region 2). The nanoclusters formed in Region 1 were spherical and monodisperse, and their size and shape remained unchanged even at higher pressures and temperatures (see supplementary Figure S1 for more details).

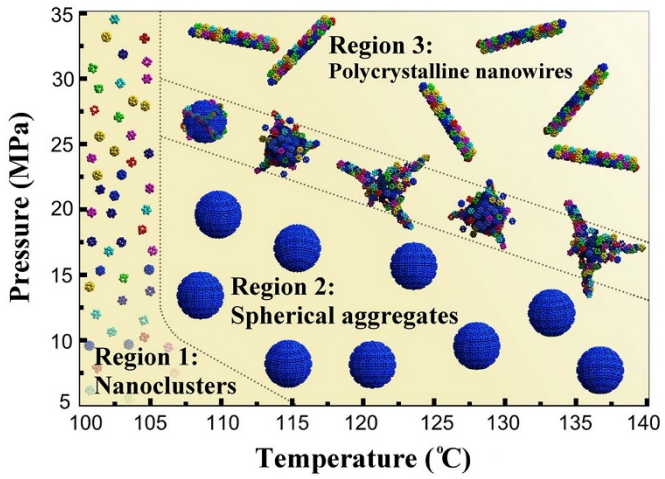

Figure 1 | P-T map showing the morphological evolution of nanomaterials under supercritical fluid condition. P-T map with a panoramic view of Gd-CeO_2 nanomaterial formation in the absence of functional capping agents or catalyst seeds.

The nanoclusters formed in Regions 2 and 3 assembled into spherical aggregates that then transformed into nanowire bundles, as shown in Fig. 2c.

Formation of nanoclusters and aggregates. Figure 3 shows TEM images of the Gd-CeO_2 nanoclusters and single-crystalline aggregates observed in Regions 1 and 2, including the selected-area diffraction (SAD) pattern and fast Fourier transform (FFT) patterns in the inset. The nanoclusters include a stable Gd-CeO_2 phase with a face-centred cubic fluorite structure (average size: 3 nm), as indicated by the dotted circles in Fig. 3a, and are highly crystalline, as indicated by the sharp ring pattern in the inset of Fig. 3a. The HRTEM images and FFT patterns in Fig. 3b indicate that individual nanoclusters comprise a single-crystalline Gd-CeO_2 phase. TEM and HRTEM images (Fig. 3c–f) acquired from specific regions on each aggregate revealed that the aggregates have many nanosized terraces at their surfaces. Although the aggregates comprised single-crystalline CeO_2, they were loosely packed as evidenced by the broad spots in the FFT patterns (inset of Figs. 3d, f). A unique contrast indicative of a 3-nm cluster was observed in the HRTEM images (indicated by dotted circles in Fig. 3d), strongly suggesting that the growth of seed-free single-crystalline aggregates in the supercritical fluid is preceded by the coalescence of the nanoclusters, which leads to the morphological change from nanoclusters to a loose single-crystalline aggregate.

Dissociation of aggregates. Figure 4 shows the initial aggregate dissociation mechanism in the transition region (Region 2 → Region 3 in Fig. 1). The internal microstructure of the aggregates (Figs. 4a, b) revealed a loosely packed single-crystalline structure comprising 3-nm nanoclusters (indicated by arrows). However, the surface of the aggregates (Figs. 4c, d) had dissociated nanoclusters (indicated by dotted circles) that served as building blocks for the growth and dissociation of aggregates in the supercritical fluid phase. During dissociation, nanoclusters could not be dissociated into atoms because of the inability of the large CO_2 molecules (diameter: 3.87 Å) to diffuse into the cluster lattice (largest (111) d-spacing of CeO_2: 3. 12 Å). Thus, HRTEM observations of the aggregate surfaces strongly evidenced the dissociation-driven morphological transition from aggregates to nanowires between Regions 2 and 3 in the P-T map.

Random growth of polycrystalline nanowires. At high temperatures and pressures, efficient CO_2 permeance into the aggregates led to the formation of nanowire bundles (Fig. 5). Nanowires were present inside the aggregates (indicated by white lines in the defocused TEM images (Figs. 5a, b) but not outside the aggregates; well-developed nanowire bundles grew on the surface of the aggregates (Figs. 5c, d). These observations confirmed that the nanowires begin to grow inside the aggregates and then propagate to the exterior.

The crystallographic images in Fig. 6 illustrate how individual nanowire bundles sprout from an aggregate. A randomly oriented polycrystalline structure comprising nanoclusters without any specific growth direction could be seen at the aggregate/nanowire sprout junction (Figs. 6b, c). However, the region marked by rectangle d in Fig. 6a (magnified image shown in Fig. 6d) revealed the original single-crystal structure. The complete transformation of all single-crystalline aggregates to polycrystalline nanowire bundles (Fig. 7) clearly implied that this unusual growth process is attributable to the dissociation and reconstruction of nanoclusters. The nanowire bundles were well separated into individual nanowires (diameter: ~20 nm; length: ~10 μm) by ultrasonic impact. The nanowire bundles (Figs. 7b, c) comprised several polycrystalline nanowires, each of which included randomly aligned nanoclusters that serve as the building blocks for nanowire assembly.

Discussion

Figure 8 schematically summarizes the mechanism underlying the unique nanoparticle-to-polycrystalline-nanowire transition (see Supplementary Movie 1). While the formation mechanisms for nanoclusters and single-crystalline aggregates were similar to those reported previously[37], the mechanism of polycrystalline nanowire growth beyond Region 2 was different. The nanoclusters formed by dissolution and precipitation of the precursors (Fig. 8a) underwent collision and coalescence in the supercritical fluid to yield aggregates with intercluster interfaces. The nanoclusters in the aggregates aligned themselves into a single crystal such that the interfacial

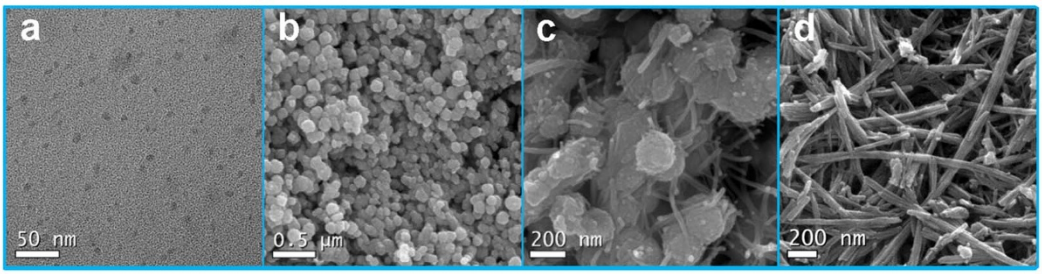

Figure 2 | SEM/TEM details of the morphological evolution of nanomaterials with variations of pressure and temperature. (a) Nanoclusters (Region 1). (b) Spheroidal aggregates (Region 2). (c) Aggregates with nanowire sprouts (transition region between Regions 2 and 3). (d) Nanowires (Region 3).

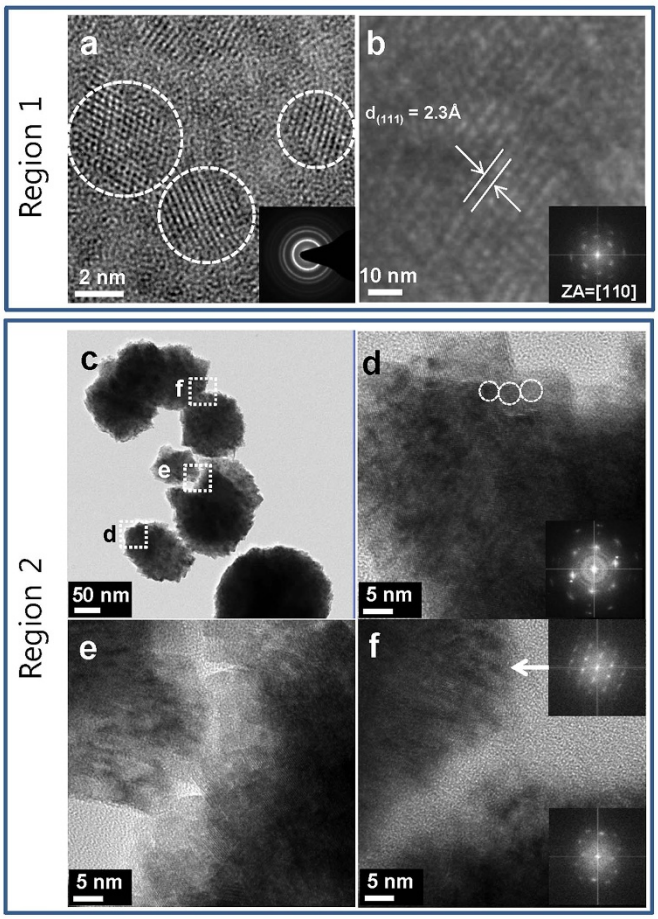

Figure 3 | TEM images and diffraction patterns of nanoclusters and single-crystalline aggregates in Region 1 and 2. (a) HRTEM image of Gd-CeO_2 nanoclusters (average diameter: 3 ± 0.5 nm) with high crystallinity, as revealed by the sharp diffraction rings in the inset. (b) HRTEM image and FFT pattern showing the fcc crystal structure of individual nanoclusters. (c) Aggregates. (d), (e), and (f) Enlarged HRTEM images and FFT patterns. In Region 2, all the TEM observations indicate that the single-crystalline aggregates comprised loosely aligned nanoclusters.

energy was minimized, and they eventually formed a loosely packed structure (similar to a mosaic structure, Region 2 in Fig. 8b).

In the transition region and Region 3, the balance between the interfacial energy of the nanoclusters in the aggregates and the permeance of CO_2 should be considered. The interfacial energy decreases markedly with an increase in pressure and temperature because the liquid/solid interfacial tension becomes almost zero under the supercritical conditions[30]. Thus, the penetrating force is more dominant than the interfacial energy. As a result, the single-crystalline aggregates dissociate into nanoclusters (Fig. 8c) and reassemble to form polycrystalline nanowires inside and outside the aggregates (Figs. 8d, e). While the formation of polycrystalline nanowires by the random alignment of nanoclusters in the absence of functional capping agents and catalyst seeds leading to self-aligned growth of nanowires is established, it is difficult to provide a thermodynamic explanation for the growth mechanism (see Figure S2 for the kinetic details controlled with time). The random orientation of the polycrystalline nanowires implies non-selective attachment of CO_2 molecules on arbitrary crystal planes of the nanoclusters in the metastable transition region. The fusion of the uncapped regions of the nanoclusters is energetically favourable as this reduces the difference in surface energy between the nanoclusters and facilitates the

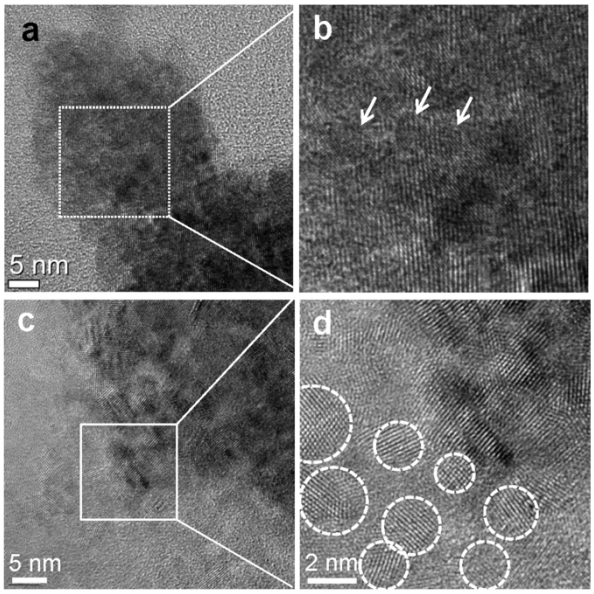

Figure 4 | HRTEM images of the interior and exterior of the dissociated aggregates at the early stage of the transition. (a) Aggregates. (b) Single-crystal lattice image at the interior of the dissociated aggregates, with clear contrast due to the nanoclusters (see arrows). (c) and (d) HRTEM images of nanoclusters dissociating at the aggregate surface.

formation of polycrystalline nanowires (Fig. 8f). Thus, supercritical CO_2 is confirmed to be the appropriate medium for the growth of polycrystalline nanowires.

In summary, the formation of Gd-CeO_2 nanomaterials such as nanoclusters, aggregates, and nanowires in a supercritical CO_2-ethanol system was analysed on the basis of a P-T map divided into

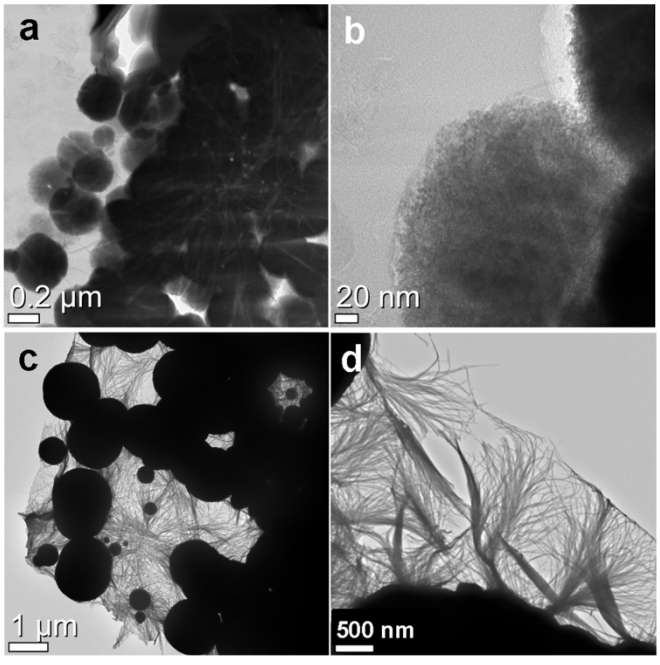

Figure 5 | TEM images of nanowires grown from aggregates at the final stage of the transition region. (a) and (b) Gd-CeO_2 nanowires grown from aggregates. Defocused TEM image showing the growth of nanowires from the interior of the aggregates. (c) and (d) Aggregates and well-developed nanowires. Nanowire bundles grow on the surface of the aggregates.

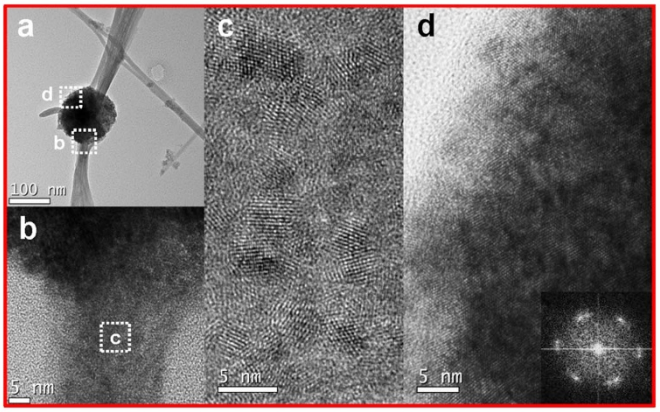

Figure 6 | TEM images showing random-alignment-based growth mechanism of polycrystalline Gd-CeO_2 nanowires. (a) A representative feature of an aggregate with nanowire sprouts. (b) Individual nanocluster is reconstructed into a polycrystalline nanowire with non-crystallographic alignment. (c) Magnified image of b showing polycrystalline nanoclusters. (d) Aggregate surface with single-crystalline structure during nanowire growth.

three regions. The single-crystalline aggregates comprised loosely aligned nanoclusters for minimizing the high interfacial energy between the nanoclusters under low CO_2 permeance. In the transition region with higher CO_2 permeance, the aggregates dissociated into nanoclusters partially covered by CO_2, which in turn attached to one another non-selectively to afford polycrystalline nanowires. This type of reconstruction is significant in that it opens up a new nanowire fabrication route without the need for seeds or capping agents, facilitates large-scale production, and could be applied to other materials.

Methods

Synthesis of Gd-CeO_2 nanomaterials. For solvothermal crystallization using supercritical carbon dioxide, 65 mL ethanolic solutions of cerium nitrate $Ce(NO_3)_3{\cdot}6H_2O$ with 99% purity, including 20 mol% gadolinium nitrate $Gd(NO_3)_3{\cdot}6H_2O$ (concentration: 45–90 mg/mL), were fed to a 350-mL high-pressure vessel. The vessel was charged with 99.99% CO_2 at pressures of up to 7.5 MPa at 35°C and then heated for 15 min at 100–140°C and 5–35 MPa until the ethanolic solution and CO_2 reached the supercritical fluid state. Subsequently, the reaction solution was cooled to ambient temperature without water cooling, and then, the vessel was slowly depressurized for 10 min. The as-synthesized nanomaterials were collected by sedimentation, centrifuged at 1,400 × *g* (3,000 rpm) for 10 min in a 15-mL conical centrifuge tube, repeatedly washed with ethanol three times, and dried at 60°C for 12 h.

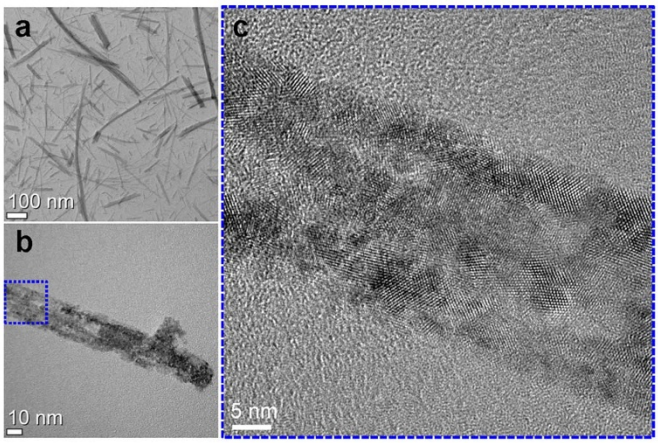

Figure 7 | TEM images of polycrystalline nanowires. (a) and (b) TEM images of nanowire bundles under different levels of magnification. (c) A nanowire bundle clearly consists of several polycrystalline nanowires with randomly aligned 3-nm nanoclusters.

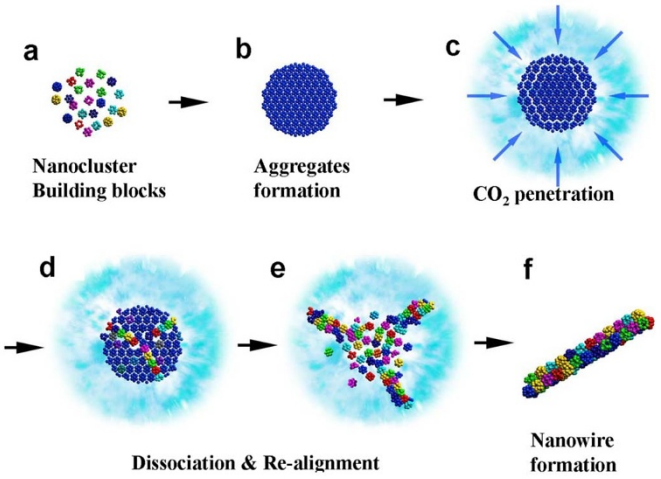

Figure 8 | Schematic diagram showing random-alignment-based growth mechanism of polycrystalline Gd-CeO_2 nanowires. (a), (b), (c), (d), (e), and (f) Schematic of the mechanism showing morphological change from nanoclusters to polycrystalline nanowires mediated by supercritical carbon dioxide. In the morphological evolutions, individual nanoclusters act as a building block of nanomaterials.

Microstructural characterization. The morphology and microstructure of the nanomaterials were examined by scanning electron microscopy (SEM, Nova NanoSEM, FEI, USA) and transmission electron microscopy (TEM, Tecnai F20, FEI, USA) as well as high-resolution TEM (HR-TEM) and energy-dispersive X-ray spectrometry (EDS, EDAX). Cryo-TEM was adopted to investigate the actual dissociation state of the aggregates. In this method, the nanomaterial solution exiting the fluid chamber was cooled to cryogenic temperatures by the Vitrobot, and a 100-nm-thick vitrified film indicative of the near in situ state during the dissociation reaction was prepared. For observing the dissociation behaviour of aggregates, in particular, we prepared the ex-situ TEM sample by putting C-coated TEM grids on the glass positioned at the centre region of the chamber.

1. Chueh, W. C., Hao, Y., Jung, W. C. & Haile, S. M. High electrochemical activity of the oxide phase in model ceria-Pt and ceria-Ni composite anodes. *Nature Mater.* **12**, 1–7 (2011).
2. Murray, E. P., Tsai, T. & Barnett, S. A. A direct-methane fuel cell with a ceria-based anode. *Nature Lett.* **400**, 649–651 (1999).
3. Wang, Y. G., Zhang, L. C. & Biddut, A. Chemical effect on the material removal rate in the CMP of silicon wafers. *Wear* **270**, 312–316 (2011).
4. Moos, R. *et al.* Resistive oxygen gas sensors for harsh environments. *Sensors* **11**, 3439–3465 (2011).
5. Liu, L. *et al.* Morphology and nanosize effects of ceria from different precursors on the activity for NO reduction. *Catalysis Today* **175**, 48–54 (2011).
6. Zhou, K., Wang, X., Sun, X., Peng, Q. & Li, Y. Enhanced catalytic activity of ceria nanorods from well-defined reactive crystal planes. *J. Catalysis* **229**, 206–212 (2005).
7. Georgi, N. *et al.* Support nanostructure boosts oxygen transfer to catalytically active platinum nanoparticles. *Nature Materials* **10**, 310–315 (2011).
8. Ji, Z. *et al.* Designed synthesis of CeO_2 nanorods and nanowires for studying toxicological effects of high aspect ratio nanomaterials. *ACS Nano* **6**, 5366–5380 (2012).
9. Xing, X. R. *et al.* Facile alcohothermal synthesis of large-scale ceria nanowires with organic surfactant assistance. *Physica B* **390**, 59–64 (2007).
10. Yan, R. X., Gargas, D. & Yang, P. D. Nanowire Photonics. *Nat. Photonics* **3**, 569–576 (2009).
11. Borgstrom, M. T., Immink, G., Ketelaars, B., Algra, R. & Bakkers, E. P. A. M. Synergetic nanowire growth. *Nature Nanotech.* **2**, 541–544 (2007).
12. Yuan, Z. Y., Vantomme, A., Du, G. H. & Su, B. L. Surfactant-assisted large-scale preparation of crystalline CeO_2 nanorods. *Langmuir* **21**, 1132–1135 (2005).
13. Wang, N., Cai, Y. & Zhang, R. Q. Growth of nanowires. *Mater. Sci. Eng. R* **60**, 1–51 (2008).
14. Yada, M. *et al.* H. Cerium compound nanowires and nanorings templated by mixed organic molecules. *Adv. Mater.* **16**, 1222–1226 (2004).
15. Lin, H. L., Wu, C. Y. & Chiang, R. K. Facile synthesis of CeO_2 nanoplates and nanorods by [100] oriented growth. *J. Colloid Interface Sci.* **341**, 12–17 (2010).
16. Lu, W. & Lieber, C. M. Nanoelectronics from the bottom up. *Nat. Mater.* **6**, 841–850 (2007).

17. Qin, Y., Wang, X. D. & Wang, Z. L. Microfibre-nanowire hybrid structure for energy scavenging. *Nature* **451**, 809–813 (2008).
18. Hochbaum, A. I. *et al*. Enhanced thermoelectric performance of rough silicon nanowires. *Nature* **451**, 163–167 (2008).
19. Patolsky, F. *et al*. Detection, stimulation, and inhibition of neuronal signals with high-density nanowire transistor arrays. *Science* **313**, 1100–1104 (2006).
20. Wang, X. D., Song, J. H., Liu, J. & Wang, Z. L. Direct-current nanogenerator driven by ultrasonic waves. *Science* **316**, 102–105 (2007).
21. Yang, R. S., Qin, Y., Dai, L. M. & Wang, Z. L. Power generation with laterally packaged piezoelectric fine wires. *Nat. Nanotechnol.* **4**, 34–39 (2009).
22. Law, M. *et al*. Nanoribbon waveguides for subwavelength photonics integration. *Science* **305**, 1269–1273 (2004).
23. Beckman, R., Johnston-Halperin, E., Luo, Y., Green, J. E. & Heath, J. R. Bridging dimensions: Demultiplexing ultrahigh-density nanowire circuits. *Science* **310**, 465–468 (2005).
24. Hu, Y. J. *et al*. A Ge/Si heterostructure nanowire-based double quantum dot with integrated charge sensor. *Nat. Nanotechnol.* **2**, 622–625 (2007).
25. Tian, B. Z. *et al*. Coaxial silicon nanowires as solar cells and nanoelectronic power sources. *Nature* **449**, 885–890 (2007).
26. Law, M., Greene, L. E., Johnson, J. C., Saykally, R. & Yang, P. D. Nanowire dye-sensitized solar cells. *Nat. Mater.* **4**, 455–459 (2005).
27. Kuykendall, T., Ulrich, P., Aloni, S. & Yang, P. Complete composition tunability of InGaN nanowires using a combinatorial approach. *Nat. Mater.* **6**, 951–956 (2007).
28. Huang, P. X. *et al*. CeO_2 nanorods and gold nanocrystals supported on CeO_2 nanorods as catalyst. *J. Phys. Chem. B.* **109**, 19169–19174 (2005).
29. Zhou, K. *et al*. enhanced catalytic activity of ceria nanorods from well-defined reactive crystal planes. *J. Catalysis* **229**, 206–212 (2005).
30. Shah, P. S. *et al*. Nanocrystal and nanowire synthesis and dispersibility in supercritical fluids. *J. Phys. Chem. B* **108**, 9574–9587 (2004).
31. Hanrath, T. & Korgel, B. A. Supercritical fluid-liquid-solid (SFLS) synthesis of Si and Ge nanowires seeded by colloidal metal nanocrystals. *Adv. Mater.* **15**, 437–440 (2003).
32. Holmes, J. D. *et al*. Control of thickness and orientation of solution-grown silicon nanowires. *Science* **287**, 1471 (2000).
33. Wen, J. G. *et al*. Self-assembly of semiconducting oxide nanowires, nanorods, and nanoribbons. *Chem. Phys. Lett.* **372**, 717–722 (2003).
34. Lin, K. S. & Chowdhury, S. Synthesis, characterization, and application of 1-D cerium oxide nanomaterials: A review. *Int. J. Mol. Sci.* **11**, 3226–3251 (2010).
35. Yang, P., Yan, R. & Fardy, M. Semiconductor nanowire: What's next? *Nano Lett.* **10**, 1529–1536 (2010).
36. Lee, J. M., Ahn, J. P. & Kim, S. W. Growth of nanostructured polycrystalline cerium oxide through a solvothermal precipitation using near-supercritical fluids. *J. Nanosci. Nanotech.* **10**, 130–134 (2010).
37. Cansell, F., Aymonier, C. & Loppinet-Serani, A. Review on materials science and supercritical fluids. Current opinion in solid state and materials. *Science* **7**, 331–340 (2003).

Acknowledgments

We gratefully acknowledge the financial support from the Ministry of Knowledge Economy and the partial support extended by the Korea Institute of Science and Technology. This research was supported by the Pioneer Research Center Program through the National Research Foundation of Korea funded by the Ministry of Education, Science and Technology (2011-0002342).

Author contributions

S.W. and J.P. contributed equally to this work by conceiving and discussing the project.

Additional information

Supplementary information accompanies this paper at http://www.nature.com/scientificreports

Competing financial interests: The authors declare no competing financial interests.

How to cite this article: Kim, S.W. & Ahn, J.-P. Polycrystalline nanowires of gadolinium-doped ceria via random alignment mediated by supercritical carbon dioxide. *Sci. Rep.* **3**, 1606; DOI:10.1038/srep01606 (2013).